Chemical Engineering Journal 525 (2025) 169895

Contents lists available at ScienceDirect

Chemical Engineering Journal

journal homepage: www.elsevier.com/locate/cej

Comparing thermodynamic equilibrium isotherms, mechanistic kinetic models and mass transfer resistances for fixed bed CO_2 direct air capture (DAC)

Dana Marinič [a,b], Žan Lavrič [a], Matej Huš [a,c], Janvit Teržan [a], Blaž Likozar [a,b,*]

[a] Department of Catalysis and Chemical Reaction Engineering, National Institute of Chemistry, Hajdrihova 19, 1000, Ljubljana, Slovenia
[b] Faculty of Chemistry and Chemical Engineering, University of Maribor, Smetanova ulica 17, 2000, Maribor, Slovenia
[c] Association for Technical Culture of Slovenia (ZOTKS), Zaloška 65, 1000, Ljubljana, Slovenia

ARTICLE INFO

Keywords:
Direct air capture
Intrinsic adsorption kinetics
CO_2 breakthrough modeling
Amine-functionalized sorbents
Lewatit® VP OC 1065
Density functional theory

ABSTRACT

The dynamic behavior of CO_2 adsorption in fixed-bed systems is critical for the design and optimization of efficient adsorption-based separation processes. This study focuses on dilute CO_2 adsorption (400–2000 ppm) onto Lewatit® VP OC 1065, under ambient and sub-ambient temperature conditions (−10 to 40 °C), which are particularly relevant for direct air capture but often overlooked in the literature. A one-dimensional dynamic model incorporating convection, axial dispersion, and adsorption kinetics was developed and validated against experimental breakthrough data. A thorough evaluation of all relevant isotherms and kinetic models presented in the existing literature has been conducted, and a comprehensive comparison was performed to determine which model provides the best overall performance under the specified criteria. The dual-site Langmuir isotherm combined with a pseudo-first linear driving force approach was found to best describe the system's performance. The heat of adsorption determined from the dual-site isotherm model was calculated to be −69.8 kJ mol^{-1} for the high-energy sites and −50.0 kJ mol^{-1} for the low-energy sites. The total adsorption capacity was determined to be 3.32 mmol g^{-1}, closely matching the value derived from elemental analysis. Contrary to common assumptions, the Toth isotherm did not consistently provide the best fit. Simulations were conducted using MATLAB, and the results closely matched experimental data, confirming the reliability of the modeling approach. The rate constant was determined to be 0.0061 min^{-1} at 20 °C. The estimated barrier for activated chemisorption from fitting experimental data to the model was 61.2 kJ mol^{-1}, which is consistent with ab initio atomistic modeling results. We validated our findings using density functional theory (DFT), providing a multiscale perspective that links macroscopic behavior with molecular-level interactions.

1. Introduction

CO_2 is the dominant greenhouse gas (GHG), accounting for over 82.5 % of total GHG emissions [1]. Atmospheric concentrations have risen above 420 ppm, which is over 50 % higher compared to pre-industrial levels [2]. The Intergovernmental Panel on Climate Change estimates that 100 to 1000 gigatons of net CO_2 removal will be required by the end of this century, in addition to aggressive emissions reductions [3]. Achieving this goal will likely involve a combination of various carbon dioxide removal (CDR) approaches.

Direct air capture (DAC) has emerged as a promising carbon dioxide removal (CDR) technology, addressing limitations of conventional methods by capturing CO_2 directly from the atmosphere, regardless of its source [4]. This enables on-site utilization for industrial applications, including liquid hydrocarbon fuel synthesis [5,6], beverage carbonation, or greenhouse enrichment for algae cultivation [7].

Despite the evident advantages of DAC, its adoption in the industrial sector remains limited. Out of all the CDR methods, DAC is considerably the most expensive, mainly because of high air dilution. To capture 1 mol of CO_2, 2600 mol of air need to be treated [8], necessitating the use of highly selective and energy intensive techniques. For an economically viable process, DAC must scale up to the gigaton level and achieve a cost below $100 per ton by 2050. The energy-intensive regeneration process (7–13 GJ tCO_2^{-1}) offers the greatest potential for improvement and reduction of operational costs [9].

To attain the desired outcome of cost and energy reduction within

* Corresponding author at: Department of Catalysis and Chemical Reaction Engineering, National Institute of Chemistry, Hajdrihova 19, 1000, Ljubljana, Slovenia.
E-mail address: blaz.likozar@ki.si (B. Likozar).

https://doi.org/10.1016/j.cej.2025.169895
Received 15 June 2025; Received in revised form 31 August 2025; Accepted 19 October 2025
Available online 20 October 2025

the process, a fundamental requirement is process optimization, a task that can be facilitated through the utilization of various numerical models. Process simulation is increasingly used in design to cut costs by reducing the need for lab and pilot testing before scaling up. By integrating it with molecular-level simulations to create multi-scale models, it becomes possible to accelerate material screening, optimize process conditions, and better understand molecular interactions [10]. However, due to the complex nature of the process, its simulation is challenging, primarily due to the sorbent capacity dependency on ambient conditions [11].

Mathematical description of the adsorption process must capture two key aspects: equilibrium and dynamics, which encompass kinetics, as well as mass and heat transfer [12]. In fixed-bed columns, the most detailed and systematic models describing the dynamic behavior of CO_2 adsorption rely on partial differential equations governing mass balance. These equations account for axial dispersion, convection, and adsorption kinetics onto the sorbent surface. The rate of adsorption establishes the link between the fluid and solid-phase mass balance equations but does not incorporate internal mass transfer limitations. It is typically represented using the Linear Driving Force (LDF) approximation, with models such as pseudo-first-order, pseudo-second-order, Avrami, or Toth kinetics. Meanwhile, equilibrium at the solid-gas interface is commonly described using adsorption isotherm models, including Langmuir, Toth, Sips, and Freundlich [13].

Several reported studies have compared various LDF models to best characterize the intrinsic kinetics. Among pseudo-first-order, pseudo-second-order, and Avrami models, the Avrami model was found to be the most suitable for describing the experimental data for PM01 [14], PEI/SBA-15 [15], TEPA/SBA-15 [15], and TRI-PE-MCM41 [16]. In another study, Bos et al. [17] compared the pseudo-first-order and pseudo-second-order LDF models to the Toth rate equation for Lewatit® VP OC 1065, with the latter showing a better fit. These studies utilized various isotherm equilibrium models to determine the equilibrium adsorption capacity in LDF models, including the Toth isotherm [17], Dual-site Toth isotherm [16], or they experimentally determined equilibrium adsorption capacity [14,15]. Moreover, Oliveira et al. [13] compared three isotherm models, Langmuir, Toth, and Sips, within a pseudo-first-order LDF model for NaY, finding that the Toth and Sips models provided the best fit to the experimental data.

Dynamic adsorption processes have been extensively studied for CO_2 capture, though less so in the context of DAC. Rigorous fixed-bed models for DAC have been developed for various amine-functionalized sorbents [18,19], including amine-functionalized silica such as PEI-SiO_2 [20] and SI-AEATPMS [21], amine functionalized nano fibrillated cellulose materials [21–23], MOFs [21], and amine functionalized MOFs [24]. A mathematical model for diffusion and reaction into a spherical particle of Lewatit® VP OC 1065 observed that higher CO_2 pressures increased the adsorption rate, though the study focused on CO_2 concentrations between 5 and 20 % in N_2, with activation energies ranging from 15 to 40 kJ mol^{-1} [17]. Driessen et al. [25] further developed a nonequilibrium adsorption model based on an effectiveness factor as a function of the Thiele modulus. The factor considers internal mass transfer and intrinsic adsorption kinetics hence bypassing the need for a fully coupled particle-reactor model. Schellevis et al. [26] developed a 1D dynamic fixed-bed model of the kg-scale TVSA process in order to determine the influence of operational parameters and weather conditions on the process performance, namely energy duty and CO_2 productivity. Their study showed that, perhaps counterintuitively, maximizing the desorption temperature was essential, given sorbent stability constraints. They also found that energy expenditure could potentially decrease to as low as 20 MJ kg^{-1} CO_2 at a regeneration temperature of 120 °C, with adsorption at low temperatures primarily controlled by reaction kinetics. Additionally, increasing velocity did not notably improve the adsorption rate or mass transfer.

To advance the assessment of the Temperature Swing Adsorption (TSA) process, a comprehensive mathematical model is needed to accurately describe the adsorption behavior of materials under different conditions, such as CO_2 partial pressures and operating temperatures. While multiple models are available and have been studied independently, a thorough comparative analysis to identify the most effective one remains lacking. Different models are rarely applied to the same dataset for direct comparison. Moreover, Bos et al. [17] observed that isotherms underpredict adsorption capacity at temperatures below 20 °C. However, most studies presented in the literature are conducted at elevated temperatures (e.g., 40 °C and above), which are not representative of ambient conditions relevant to DAC. Lower temperatures are generally preferred for adsorption due to more favorable kinetics and increased CO_2 uptake.

This study aims to systematically compare various LDF models incorporating different isotherm formulations, all applied to the same dataset across a range of low to moderate temperatures under dry conditions. By doing so, we seek to identify the most accurate and robust modeling approach for predicting CO_2 adsorption. Water–CO_2 co-adsorption isotherms for this system have not yet been thoroughly explored, and including them could introduce uncertainties that mask differences between models. Dry conditions were therefore selected to allow a clear and direct comparison, enabling the most accurate and robust model to be identified. The chosen equilibrium and mass transfer descriptions were then implemented in a one-dimensional dynamic framework, accurately predicting concentration profiles in both gas and adsorbed phases. This approach allowed the adsorption and desorption kinetics to be clearly characterized.

2. Materials and methods

2.1. Materials

In this study we used commercially available supported-amine sorbent, Lewatit® VP OC 1065 purchased by Sigma Aldrich (Germany). The sorbent is an ion exchange resin, macroporous in nature and spherical bead in form [27]. It has a primary benzylamine group that reacts with CO_2. The benzylamine group is supported on a polystyrene backbone crosslinked with 8–10 % divinylbenzene [17]. The amount of benzylamine groups attached to polystyrene based ion exchange resin was determined to be 7.5 mol kg^{-1} [28]. The sorbent in a spherical shaped bread has a surface area of 43 m^2 g^{-1}, an average pore volume of 0.27 cm^3 g^{-1}, an average pore radius of 25 nm and particle size of 0.3–1.25 mm [29]. The particle density and fixed-bed voidage was reported to be 861 kg m^{-3} and 0.382 m^3 m_r^{-3}, respectively [30]. The maximum stable operating temperature assured by the manufacturer is 100 °C. However, a study conducted by Yu et al. [31] suggests that sorbent demonstrates thermal long-term stability up to 150 °C, but beyond this temperature, it undergoes thermal degradation.

2.2. Fixed-bed experiments

Temperature programmed adsorption and desorption cycles were carried out using the Micrometrics AutoChem II Chemisorption Analyser (Micrometrics, Norcross, GA, USA). The original setup was modified by adjusting the analysis valve (Fig. 1) to achieve zero-retention breakthrough. Approximately 0.1 g of wet sorbent was loaded into the column with the radius of 1 cm and length of 15 cm. A packed bed was selected for DAC modeling for its high contact area and established design, though a detailed modeling comparison with a monolith structure was performed [32].

The fixed-bed breakthrough experiments consisted of three stages. Before the first measurement, the sorbent was regenerated in pure Ar (70 ml min^{-1}, 5.0, Messer, Bad Soden am Taunus, Germany) at 100 °C until all pre-adsorbed CO_2 and water were removed. This cleaning step reduced the sorbent mass by 48.1 % compared to the wet state, as determined by TGA (Fig. S1). Adsorption tests were then performed at temperatures between −10 °C and 60 °C using a CO_2/He gas mixture

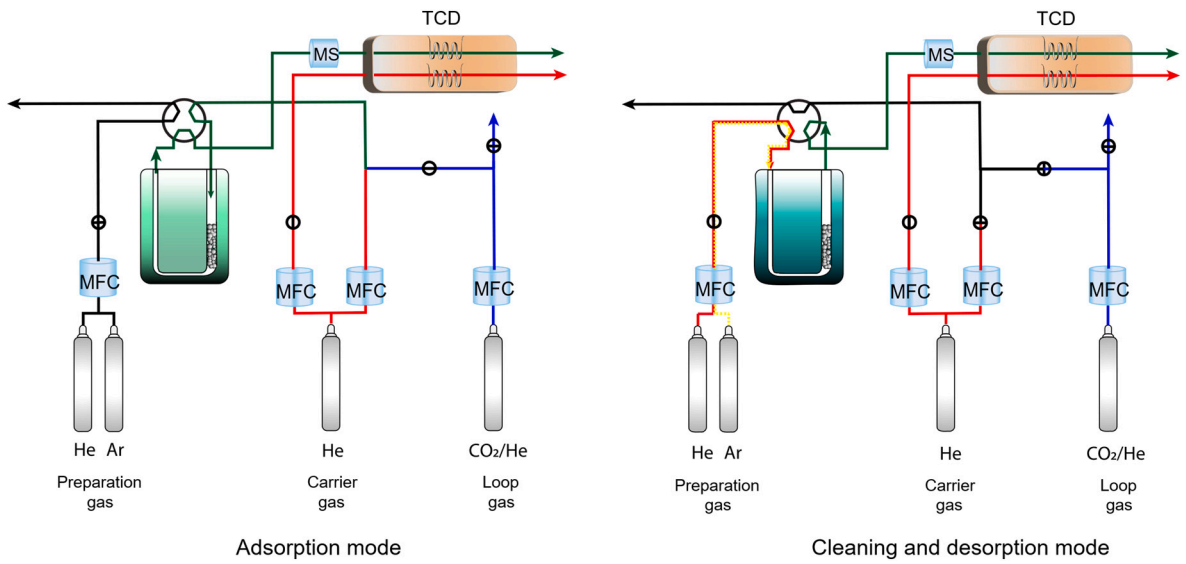

Fig. 1. Schematic representation of the experimental setup for pretreatment, CO_2 adsorption and desorption in a packed bed column using the Micrometrics AutoChem II Chemisorption Analyser.

(400–2000 ppm for breakthrough adsorption experiments, 5–75 % for adsorption equilibrium isotherms). Adsorption continued until the outlet concentration matched the inlet, indicating sorbent saturation, and could take up to 400 min. After adsorption, the system was purged with helium to remove residual CO_2. Desorption was carried out in a helium flow (70 ml min^{-1}) at 80–100 °C until full regeneration. The sorbent was reused for multiple cycles. Based on Veneman et al. [33], who reported no capacity loss under similar conditions (90–120 °C in nitrogen over 300 h), we assumed sorbent degradation had no significant impact on our results. The reactor outlet gases were monitored by mass spectrometer (MS) and thermal conductivity detector (TCD). All experiments were performed in duplicate to ensure reproducibility, and reported loadings represent the average of both measurements.

The equilibrium CO_2 loading (q^*) was determined by conducting a mass balance, where the accumulation term can be calculated using the following equation:

$$\int_0^\infty \left(\frac{P_{avg}\, y_{CO2,in}\phi}{RT}\right) dt - \int_0^\infty \left(\frac{P_{avg}\, y_{CO2,out}\phi}{RT}\right) dt = q^*\, m_{\text{sorbent}} \quad (1)$$

The flow rate is denoted by ϕ, y_{CO2} refers to the CO_2 mole fraction, T is the temperature, R is universal gas constant and m_{sorbent} is the mass of dry Lewatit® VP OC 1065. The average pressure within the column (P_{avg}) was used due to the negligible pressure drop.

2.3. Ab initio modeling

Reactivity of the sorbet on the atomistic level was studied using the density functional theory (DFT) in the LCAO approach, as implemented in Gaussian 16 Revision C.02 [34]. The calculations were performed with a hybrid Minnesota functional M06-2X [35], which performs particularly well for main group thermochemistry and kinetics. It also accounts for non-covalent interactions [36], which are important for the initial physisorption of CO_2. Due to the size of the system, a moderately large 6-311G(d,p) basis set had to be used [37]. A heptameric fragment was chosen to account for the size and complexity of the sorbent and effects of adjacent amino groups, rather than increasing the basis set or level of theory on a smaller structure. Due to a relatively flat potential energy surface, several initial geometries were probed, optimized, perturbed and re-optimized. Observing that the energetics is dominated by the number of hydrogen bonds among the amino groups, the structure with the most hydrogen bonds was ultimately chosen. Special care was taken to maintain the same conformation during the computations, i.e. to ensure that the energy changes stem from the chemical transformations at the reaction site and not configurational changes.

Enthalpic and entropic corrections to the Gibbs free energy included the vibrational, rotational and translation contributions for gaseous species and vibrational contribution only for adsorbed species. Transition states were identified using the transit-guided quasi-Newton (STQN) method and confirmed to have precisely one imaginary frequency [38].

The polymer structure of the amine sorbent (Lewatit® VP OC 1065) was modeled as a heptamer of (aminomethyl)styrene units, as shown in Fig. 2. A molecule of CO_2 can then interact with the amine groups through van der Waals interactions. Chemisorption, however, is achieved through covalent bonding, which forms a carbamate.

2.4. Isotherm models

The adsorption equilibrium of CO_2 on sorbent material is typically described by isotherm models. These models relate the partial pressure of the adsorbate in the gas phase (P_{CO_2}) to the adsorption capacity on the solid surface at the equilibrium (q^*). The CO_2 capacities were calculated by integrating the relevant sections of the dynamic breakthrough curves. The data were fitted using several established isotherm models to compare their performance.

The first isotherm model studied was the Langmuir model (Eq. (2)). Due to the several Langmuir limitations, particularly its restriction to homogeneous systems, the Toth isotherm (Eq. (3)) was empirically derived to better fit experimental data. Unlike models based on first principles, it adjusts the Langmuir model to account for sub-monolayer

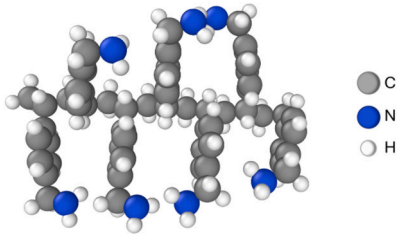

Fig. 2. Atomistic model of the amine sorbent as a heptamer of (aminomethyl) polystyrene.

coverage and surface heterogeneity through empirical parameter t_h. While other semi-empirical models, such as Freundlich and Sips, struggle to describe adsorption behavior at low and/or high CO_2 partial pressures, the Toth isotherm effectively captures adsorption across all pressure ranges [39].

$$q^* = \frac{q_s b P_{CO_2}}{1 + bP_{CO_2}} \tag{2}$$

$$q^* = \frac{q_s b P_{CO_2}}{\left(1 + (bP_{CO_2})^{t_h}\right)^{1/t_h}} \tag{3}$$

Here, q_s presents the maximum adsorption capacity and the parameter b is the isotherm constant specific for adsorbate-adsorbent accounting for the adsorption affinity. Both b and q_s are temperature-dependent and can be expressed as:

$$b = b_\infty \cdot \exp\left(-\frac{\Delta H_{ADS}}{RT}\right) = b_0 \cdot \exp\left(\frac{\Delta H_0}{RT_0}\left(\frac{T_0}{T} - 1\right)\right) \tag{4}$$

$$q_s = q_{s0} \cdot \exp\left(\chi\left(1 - \frac{T}{T_0}\right)\right) \tag{5}$$

$$t_h = t_{h0} + \alpha\left(1 - \frac{T_0}{T}\right) \tag{6}$$

where ΔH_{ADS} is the heat of adsorption and ΔH_0 corresponds to the isosteric heat of adsorption at zero coverage. The parameters b_0 and b_∞ represent the adsorption affinity at the reference temperature and infinite temperature, respectively. Along with q_{s0}, these parameters serve as the model's reference values at the reference temperature T_0. χ is the dimensionless parameter. Similar to parameter b, t_h is also specific to the adsorbate-adsorbent pair. There is no strong theoretical justification for the parameter and it can be given in the form presented in Eq. (6), where t_{h0} corresponds to Toth model reference parameter and α is the dimensionless parameter.

Guerrero et al. [40] introduced a Dual-Site Langmuir model (Eq. (7)) that considers two types of adsorption sites with distinct adsorption energies. The model distinguishes between high-energy sites, which have a greater affinity for adsorbate molecules, and low-energy sites. The model separates the adsorption mechanisms into two terms: one for chemisorption by amine groups and the other for physisorption through surface interactions [4].

$$q^* = \frac{q_{s,1} b_1 P_{CO_2}}{1 + b_1 P_{CO_2}} + \frac{q_{s,2} b_2 P_{CO_2}}{1 + b_2 P_{CO_2}} \tag{7}$$

2.5. Linear driving force models

Reaction rate equations characterize the intrinsic kinetics of CO_2 adsorption on the sorbent surface but are not accounting for mass transfer limitations [17]. Different linear driving force (LDF) models are used to describe adsorption behavior. Given that a high adsorption rate is a critical parameter in the DAC process, directly influencing the adsorber size and, consequently, the overall cost, it is essential to study and optimize this aspect [11].

The pseudo-first-order LDF model (Eq. (8)), originally proposed by Lagergren [41], is the simplest and widely used model in many fields of research. It describes the adsorption rate $\left(\frac{\partial q}{\partial t}\right)$ as being proportional to the number of vacant adsorption sites. However, in cases where two functional groups are required to capture a single CO_2 molecule, such as in dry amine-based sorbents, the pseudo-second-order model (Eq.(9)) is more appropriate from a mechanistic perspective [17]. The Avrami model, initially developed to describe particle nucleation kinetics [42], has also been applied to CO_2 adsorption on amine-functionalized sorbents (Eq. (10)). The only mechanistically derived LDF model is Langmuir model (Eq. (11)), whereas others assume a simple empirical approach. The Toth LDF model (Eq. (12)) is a modified version of the Langmuir model to better account for surface heterogeneity [43].

$$\frac{\partial q}{\partial t} = k_{LDF,1}(q^* - q) \tag{8}$$

$$\frac{\partial q}{\partial t} = k_{LDF,2}(q^* - q)^2 \tag{9}$$

$$\frac{\partial q}{\partial t} = k_{LDF,A}^{nA} t^{nA-1}(q^* - q) \tag{10}$$

$$\frac{\partial q}{\partial t} = k_{\text{Lang}}\left\{P_{CO_2}\left[1 - \left(\frac{q}{q_s}\right)\right] - \frac{1}{b}\frac{q}{q_s}\right\} \tag{11}$$

$$\frac{\partial q}{\partial t} = k_{\text{Toth}}\left\{P_{CO_2}\left[1 - \left(\frac{q}{q_s}\right)^{t_h}\right]^{\frac{1}{t_h}} - \frac{1}{b}\frac{q}{q_s}\right\} \tag{12}$$

In the equations, q represent the loading at the time t, while k denotes the kinetic constant. The subscripts indicate the specific model to which each constant belongs. The Avrami exponent, nA, accounts for changes in the adsorption mechanism. The equilibrium loading (q^*) is determined as outlined in Section 2.4 [44].

The kinetic constants (k) are calculated based on the linear form of Arrhenius equation:

$$k = k_0 \exp\left(\frac{E_a}{R}\left(\frac{1}{T_0} - \frac{1}{T}\right)\right) \tag{13}$$

where k_0, E_a, and T_0 are the pre-exponential factor, activation energy, and reference temperature, respectively.

2.6. Dynamic model for fixed bed reactor

The adsorption model describing the temperature swing adsorption cycle incorporates the transient gas phase component mass balance, accounting for accumulation in the fluid phase, convection flow term, axial dispersion, and the kinetics of both adsorption and desorption [45]:

$$\frac{\partial C_b}{\partial t} = -v_z \frac{\partial C_b}{\partial z} + D_{ax}\frac{\partial^2 C_b}{\partial z^2} - \frac{(1 - \varepsilon_b)\rho_p}{\varepsilon_b}\frac{\partial q}{\partial t} \tag{14}$$

Here, C_b, D_{ax}, v_z, ε_b, ρ_p present the total gas concentration in the bulk phase, axial dispersion coefficient, gas phase interstital velocity, bed porosity, and particle density, respectively. The mass transfer kinetics is defined using the LDF approximations through rate equations ($\frac{\partial q}{\partial t}$), which establish a link between the fluid and solid-phase mass balance equations, as shown in Eqs. (8)–(12).

The model is developed by first applying the Finite Element Method for spatial discretization, which divides the domain into manageable elements. At each time step, time integration is carried out using backward differentiation formulas for the first derivative, with solutions at each step relying on the previous interval's data, and central finite differences for the second derivative. This approach results in a system of nonlinear algebraic equations, which is then linearized iteratively using the Damped Newton Method. Appropriate boundary and initial conditions are defined to ensure a well-posed problem, and the resulting linear systems are solved using direct or iterative matrix solution algorithms until convergence is achieved.

To solve the differential equations, the following initial and boundary conditions were needed:

$$q(t,z) = 0, t = 0, 0 \le z \le L$$

$$C_b(t,z) = 0, t = 0, 0 \le z \le L$$

$$C_b(t,z) = c_0, t > 0, z = 0$$

$$\frac{\partial C_b}{\partial z} = 0, t > 0, z = L$$

The initial condition assumes that the gas-phase CO_2 concentration throughout the column is equal to the feed concentration at time zero, while the sorbent is initially free of CO_2. The inlet boundary condition is a constant CO_2 concentration corresponding to the feed gas, representing a well-mixed feed stream entering the column. At the outlet, a zero-gradient condition is applied, which approximates a convective exit with negligible back-diffusion. These choices are consistent with standard modeling practices for fixed-bed adsorption columns [46]. They reflect physically realistic scenarios where the column is initially empty, the feed is controlled, and the outlet does not impose artificial constraints on concentration profiles.

Isotherm, LDF and dynamic model parameters were determined by fitting the experimental data to mathematical models with the least square approximation method, where the objective function, Sum of Squared Errors of prediction (SSE), was calculated with Eq. (15):

$$SSE = \sum \left(q(t)_{exp} - q(t)_{mod} \right)^2 \quad (15)$$

In the case of fixed bed model, where concentration data was available instead of adsorption capacity, SSE was calculated using $C_b(t)_{exp}$ and $C_b(t)_{mod}$, following the same approach.

3. Results and discussion

3.1. Adsorbent characterization

Elemental composition analysis revealed that the nitrogen content of the sorbent after pretreatment was 6.1 mmol g^{-1} (Table 1). Similarly, Yu et al. [31] reported a nitrogen loading of 6.8 mol kg^{-1} for the same sorbent. Given that two amine groups are required to bind one CO_2 molecule under dry conditions, the maximum sorbent capacity (q_{s0}) was determined to be 3.05 mmol g^{-1}.

3.2. Adsorption and chemisorption mechanism

CO_2 interactions with the (aminomethyl)polystyrene predominantly through van der Waals interactions. Positioned (C—N distance) 2.7 Å from the amine group, it exhibits negligible charge density perturbation. The electronic energy of this interaction is favorable at −28.1 kJ mol^{-1} and the enthalpy is −24.8 kJ mol^{-1}, while the Gibbs free energy at 298 K and 1 atm CO_2 is unfavourable with +7.7 kJ mol^{-1}. However, a CO_2 molecule can also interact with the aromatic rings of the sorbent, although a bit more weakly with the energy, enthalpy and Gibbs free energy of −20.2 kJ mol^{-1}, −19.0 kJ mol^{-1}, and + 22.1 kJ mol^{-1}, respectively (see Fig. 3).

However, CO_2 can react with the amine group to form a carbamate moiety (R-NH-COOH). This reaction is exothermic with an electronic energy change of −96.8 kJ mol^{-1} and Gibbs free energy change of −34.4 kJ mol^{-1} at 298 K and 1 atm CO_2. Kinetically, the rate of this reaction is determined by the activation barrier. Here, the importance of modeling a sufficiently large oligomer becomes apparent. For the intramolecular reaction, where the hydrogen atom is transferred from the *same* amino group, which forms the C—N bond, the barrier is E_A = 157.2 kJ mol^{-1} ($\Delta G^{\#}$ = 180.2 kJ mol^{-1}). A high barrier is caused by a strain four-membered ring-like transition state. However, when the spatially adjacent amino group participates in the hydrogen transfer, a six-membered ring-like transition state is achieved, and the barrier is lowered to 62.7 kJ mol^{-1} ($\Delta G^{\#}$ = 91.6 kJ mol^{-1}). The Gibbs free energies are consistently larger since CO_2 adsorption entails a considerable decrease in entropy.

Table 1
Elemental composition of fresh Lewatit® VP OC 1065 after pretreatment.

w_c (%)	w_H (%)	w_N (%)	N loading (mmol g^{-1})	Ref.
81.36	8.6	8.54	6.1	This work
81.04	8.38	9.53	6.81	[31]
80.48	8.23	9.46	6.76	[31]
80.57	8.29	9.64	6.89	[31]

3.3. Adsorption equilibrium

The equilibrium adsorption capacities of the sorbent, shown as data points on the isotherms (Fig. 4), were determined from breakthrough curve data and represent the average of two independent measurements. The CO_2 partial pressures were gradually increased, and the capacities were measured at specific temperatures after the equilibrium was reached. The isothermal measurements were performed at −10, 0, 10, 20, 40 and 60 °C. The highest measured capacities were measured to be 3.4 mol kg^{-1} at lowest studied temperatures (−10 °C) and highest studied CO_2 partial pressure (0.76 bar). This exceeds the maximum sorbent capacity determined by elemental composition analysis (3.1 mol kg^{-1}), which may be attributed to experimental uncertainties. Specifically, the uncertainty in sorbent capacity derived from breakthrough experiments is estimated at ±7 % due to flow control, baseline drift, integration errors, and differences in regeneration quality. The uncertainty in maximum sorbent capacity from elemental composition analysis is estimated at ±2 % based on instrument calibration and sample preparation variability. The observed highest measured capacity slightly exceeds the maximum capacity from elemental analysis, but the difference falls within the combined experimental error. The high CO_2 equilibrium loading at low partial pressures observed in Lewatit® VP OC is a key advantage for DAC. The measured CO_2 sorbent capacity at 15 % CO_2 in He at 20 °C was 2.33 mol kg^{-1}, which is only 60 % more than in highly diluted atmosphere (400 ppm), despite the CO_2 concentration being nearly 375 times greater.

3.3.1. Langmuir isotherm model

We initially applied the Langmuir isotherm model to characterize the CO_2 adsorption equilibrium. The fitted parameters q_{s0}, b_∞ and ΔH_{ADS} are presented in Table 2.

The heat of adsorption (ΔH_{ADS}), which is equivalent to the activation energy for desorption, was determined to be 35.2 kJ mol^{-1}, confirming the exothermic nature of the process. This value agrees fairly well with the theoretically calculated enthalpy of −24.8 kJ mol^{-1}. However, it is lower than those reported by Sonnleitner et al. [47], who conducted experiments at higher temperatures (40, 60 and 95 °C), where different adsorption mechanisms may become dominant. Serna-Guerrero et al. [40] further showed that adsorption heat for Lewatit® VP OC 1065 varies with loading and temperatures, questioning the use of high-temperature data for low-temperature DAC systems.

Although the Langmuir model was inadequate in consistently describing the observed adsorption data, as evidenced by the low R^2 values (e.g., $R^2 = 0.81$), it remains a useful baseline. It is widely reported and provides the simplest approach to describing non-competitive adsorption and physically meaningful parameters. The maximum adsorption capacity (2.85 mmol g^{-1}) agreed closely with elemental analysis (3.05 mmol g^{-1}), and the affinity constant b_∞ was 1.87×10^{-10}, decreasing with increasing temperature as expected for exothermic processes [39]. However, the model could not fully capture the heterogeneity of adsorption sites, limiting its accuracy. It is only suitable for homogeneous systems where all adsorption sites are energetically identical, there are no lateral interactions between adsorbed molecules, adsorption occurs at specific and well-defined sites on the surface, and only a monolayer of adsorbate is formed.

3.3.2. Dual-site Langmuir isotherm model

In principle, any adsorption isotherm can be represented using an n-site Langmuir model. However, Buijs et al. [4] noted that a single-site

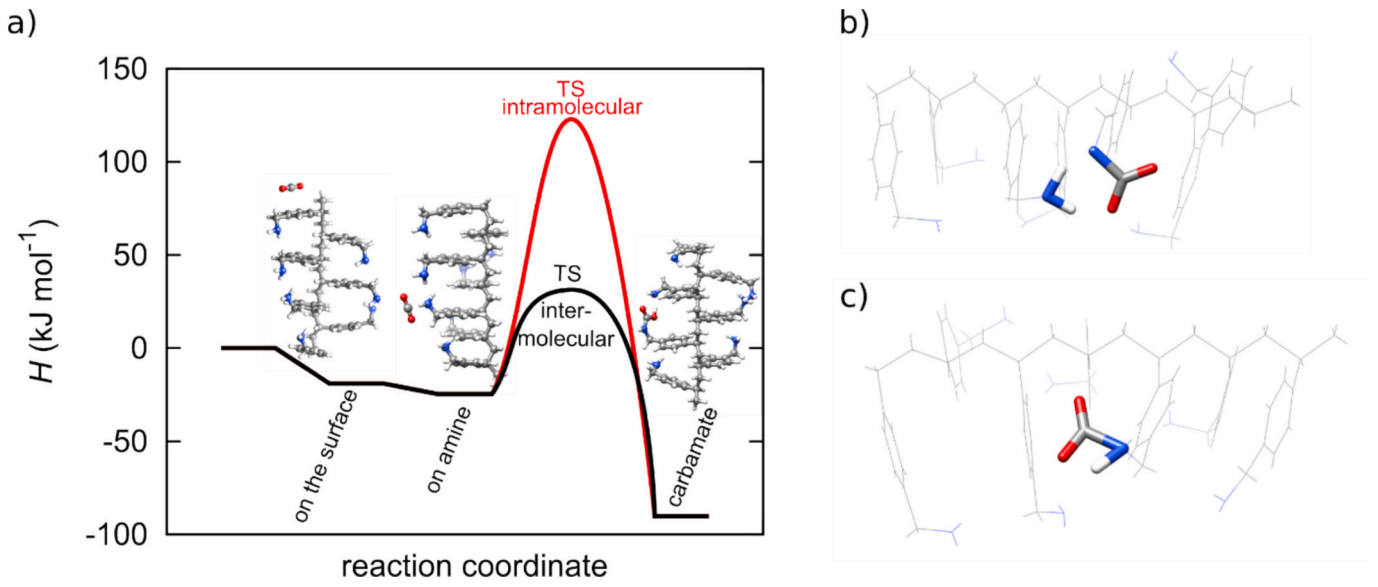

Fig. 3. a) Enthalpy of CO_2 physisorption and chemisorption on the heptamer, b) a six-membered ring-like (intermolecular) and c) four-membered ring-like (intramolecular) transition state for chemisorption. Grey spheres represent carbon atoms, red spheres represent oxygen atoms, white spheres represent hydrogen atoms and blue spheres represent nitrogen atoms.

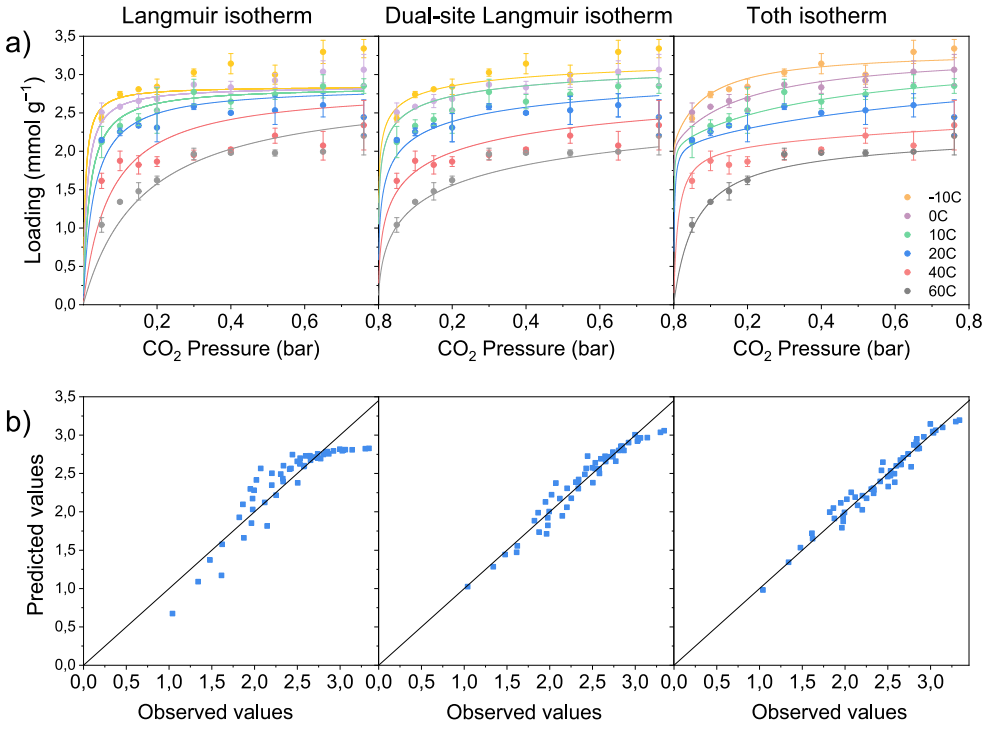

Fig. 4. a) Isotherm models (lines) and experimental data (points) of adsorption of CO_2 onto Lewatit® VP OC 1065 at −10 °C, 0 °C, 10 °C, 20 °C, 40 °C, and 60 °C. Loadings were determined from breakthrough curve data and represent the average of two independent measurements; b) Parity plots identifying the most appropriate fit by comparing the experimentally measured CO_2 adsorption capacity of the sorbent with the capacity predicted by the equilibrium model at corresponding partial pressures and temperatures.

Langmuir model is often insufficient for accurately capturing experimental data, while incorporating a third site in the model does not significantly enhance its accuracy. The fitted parameters for the Dual-site Langmuir isotherm model are presented in Table 3. As shown in Fig. 4, the model provides a good fit for the experimental data across different temperatures.

At 303 K, the total adsorption capacity, given by the sum of $q_{s0,1}$ and $q_{s0,2}$, was determined to be 3.32 mmol g^{-1}. The calculated heat of adsorption was 69.8 kJ mol^{-1} for chemisorption by amine groups and 50.4 kJ mol^{-1} for physisorption through surface interactions. These results align well with the values reported by Buijs et al. [4]. Our ab initio model shows that the enthalpy of chemisorption is 90.2 kJ mol^{-1}, and for physisorption 19.0 and 24.8 kJ mol^{-1} at the amine and aromatic sites, respectively.

To complement the parameter comparison in Tables 3, Fig. 5 provides a direct comparison between literature correlations and our

Table 2
Langmuir isotherm parameters including heat of adsorption (ΔH_{ADS}), adsorption affinity at the infinite temperature (b_∞), and maximum sorbent capacity (q_{s0}).

Symbol	This work	Sonnleitner et al. [47]	Unit
q_{s0}	2.85	2.21	mmol g^{-1}
b_∞	1.87×10^{-10}	1.17×10^{-9}	bar^{-1}
ΔH_{ADS}	35.2	65.6	kJ mol^{-1}
R^2	0.81	/	/

Table 3
Dual-site Langmuir isotherm parameters including heat of adsorption (ΔH_{ADS}), adsorption affinity at the infinite temperature (b_∞), and maximum sorbent capacity (q_{s0}).

	This work	Buijs et al. [4]	Units
$q_{s0,1}$	2.09	1.94	mol kg^{-1}
$b_{\infty,1}$	1.98×10^{-15}	1.11×10^{-15}	Pa^{-1}
$\Delta H_{ADS,1}$	−69.8	−75.6	kJ mol^{-1}
$q_{s0,2}$	1.22	1.06	mol kg^{-1}
$b_{\infty,2}$	1.14×10^{-14}	1.84×10^{-13}	Pa^{-1}
$\Delta H_{ADS,2}$	−50.4	−51.6	kJ mol^{-1}
T	303	303	K
R^2	0.96	/	/

experimental data. The results are compared with the dual-site Langmuir isotherm model from Buijs et al. [4], which was fitted to the experimental data of Veneman et al. [48], alongside our own fitted model. While both approaches yield equilibrium capacities and parameters within a similar range, small deviations are visible, reflecting the sensitivity of adsorption models to fitted parameters.

3.3.3. *Toth isotherm model*

The Toth isotherm, being a six-parameter model, provides a better fit to adsorption data compared to the Langmuir model. The parameters q_{s0}, b_0, ΔH_0, t_{h0} and α were fitted to the experimental equilibrium data at a reference temperature 293.15 K and are presented in Table 4.

Unlike the Langmuir model, which is derived from first principles, the Tóth isotherm is an empirical model that modifies the Langmuir equation to better capture real adsorption process. Although it improves the description of the data ($R^2 = 0.94$) relative to Langmuir ($R^2 = 0.81$), it does not perform as well as the Dual-Site Langmuir model ($R^2 = 0.96$). The deviation of the models from the experimental data is likely due to the absence of constraints related to limiting dynamics, such as mass transfer restrictions, chemical reaction kinetics, or sorbent deactivation by CO_2.

In the Tóth model, the heat of adsorption (ΔH_{ADS}) corresponds to the isosteric heat of adsorption at zero fractional loading (ΔH_0). The best fit to the experimental data was obtained with a value of 60.1 kJ mol^{-1}. In contrast, Veneman et al. [48] reported an isosteric heat of adsorption at zero coverage of 87 kJ mol^{-1}. Compared to previous studies, our work underestimates the adsorption capacities measured, which may be partly due to the higher temperatures typically examined in the literature. However, the heat of adsorption is known to depend on both the degree of loading and temperatures, as the latter influence surface coverage and the types of active sites involved.

The enthalpy of adsorption at a CO_2 capacity of 1.8 mol kg^{-1} was calculated to be 25.2 kJ mol^{-1} using the Clausius–Clapeyron equation [50]. In contrast, Sonnleitner et al. [47] reported a much higher value of 76 kJ mol^{-1} at the same loading and a reference temperature of 50 °C. Quantum chemical calculations predict that at higher temperatures, CO_2 starts to chemisorb as a carbamate with a reaction enthalpy of 90 kJ mol^{-1}. Similarly, Venneman et al. [48] found the enthalpy to be 75 kJ mol^{-1} at a slightly lower reference capacity of 1.5 mmol g^{-1}, however,

Table 4
Toth isotherm parameters including isosteric heat of adsorption at zero coverage (ΔH_0), adsorption affinity at the reference temperature (b_0), maximum sorbent capacity (q_{s0}), dimensionless parameters (α and χ), and Toth model reference parameter (t_{h0}).

	This work	Bos et al. [17]	Veneman et al. [48]	Sonnleitner et al. [47]	Sutanto et al. [49]	Units
q_{s0}	3.52	3.4	3.4	3.13	3.7	mol kg^{-1}
χ	0	0	0	0	0	/
b_0	2085	93	408.84	282	188.6	bar^{-1}
ΔH_0	60.1	95.3	86.7	106	111	kJ mol^{-1}
t_{h0}	0.33	0.37	0.3	0.34	0.3	/
α	0.21	0.33	0.14	0.42	0.14	/
T_0	293.15	353.15	353	343	353	K
R^2	0.94	/	/	/	/	/

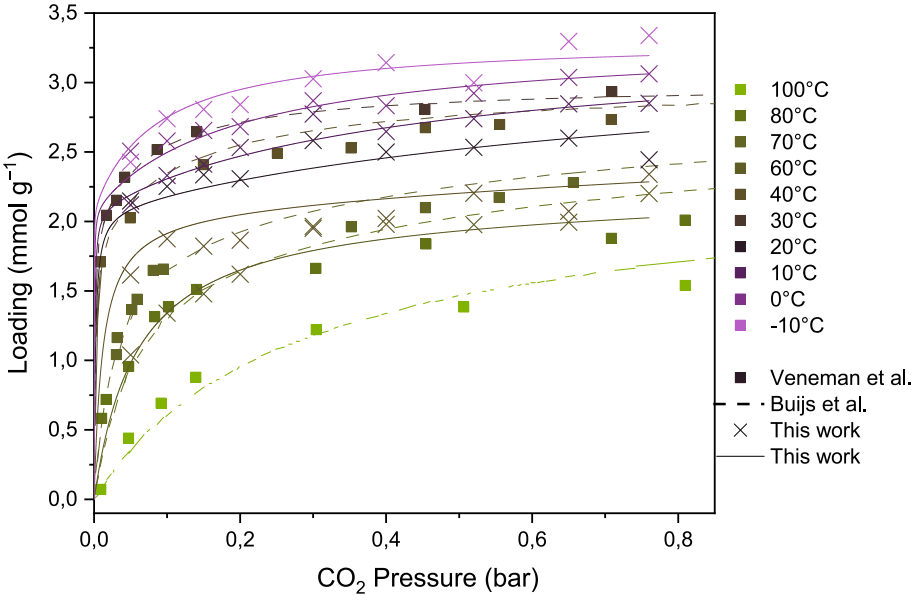

Fig. 5. Experimental equilibrium capacities from Veneman et al. [48] (squares) and this work (crosses). Dotted lines show the Dual-site Langmuir isotherm model from Buijs et al. [4] fitted to the data of Veneman et al. [49], while solid lines represent our model fitted to our experimental data.

their study also included higher temperatures ranging from 30 °C to 100 °C.

The Tóth model is expected to predict higher ΔH_0 values than the Langmuir model due to its ability to account for high-energy adsorption sites, which the Langmuir model does not distinguish. On heterogeneous surfaces, the isosteric heat of adsorption is typically higher at low coverage, as high-energy adsorption sites are occupied first. As coverage increases, ΔH decreases, reflecting the filling of lower-energy sites. The variation of ΔH with the loading for Lewatit® VP OC 1065 was proven by Serna-Guerrero et al. [40].

The heterogeneity parameter t_h is typically less than unity, with greater deviation from unity indicating a higher degree of system heterogeneity. In this study, t_{h0} was determined to be 0.33, suggesting significant surface heterogeneity. While there is no strong theoretical foundation for how t_h varies with temperature, it is generally expected to approach unity as temperature increases [39].

For this model, the parameter χ was set to zero, assuming that the maximum sorbent capacity remains independent of temperature. This assumption is reasonable, as the chemical structure of the material does not eliminate adsorption sites upon heating. However, in some amine-functionalized materials, elevated temperatures may cause amine groups and thus active sites to volatilize or become structurally distorted, thereby reducing their availability for CO_2 adsorption. The model offers flexibility to incorporate such site depletion effects in an Arrhenius-like manner if needed.

Despite these variations, the Tóth equation remains a widely preferred isotherm model due to its relatively simple form and its ability to accurately describe adsorption behavior across a range of adsorbates, including hydrocarbons, carbon oxides, hydrogen sulfide, and alcohols on both activated carbon and zeolites, at both low- and high-pressure ranges [39].

3.4. Adsorption kinetics

Four different LDF models were applied to analyze the intrinsic kinetics of CO_2 adsorption on the sorbent surface, namely pseudo-first, pseudo-second, Avrami and Toth model. Adsorption processes can be described using mechanistic or empirical approaches. While the Langmuir model is derived from fundamental principles (incorporating conservation, equilibrium, and transport kinetics), empirical models such as the pseudo-first-order and pseudo-second-order are commonly used due to their ability to fit experimental data without requiring detailed molecular mechanisms [51]. The corresponding model fits are shown in Fig. 6. The estimated kinetic and equilibrium parameters are summarized in Tables 5 and 6. Notably, incorporating the dual-site Langmuir isotherm into the pseudo-first-order kinetic model significantly improved the agreement between model predictions and experimental data. Parity plots illustrating the model performance are provided in the Supplementary Information (Fig. S2). As shown in Fig. 6, the equilibrium was reached in 100 min at 40 °C but took over 400 min at −10 °C.

3.4.1. Kinetic LDF models using Langmuir and Toth isotherm models

The LDF models exhibited some limitations in predicting CO_2 adsorption onto the sorbent. The pseudo-first and second-order models

Table 5
Kinetic model parameters, including activation energies and rate constants, for adsorption of CO_2 onto Lewatit® VP OC 1065 at $T_0 = 293.15$ K and set q_{s0}=3.05 mmol g^{-1}.

	Pseudo-first	Pseudo-second	Avrami	Toth
k_0	0.0311 min^{-1}	0.03553 mol kg^{-1} min^{-1}	0.0293 min^{-1}	107.1 mol kg^{-1} bar^{-1} min^{-1}
E_a (kJ mol^{-1})	18.8	36.4	15.7	5.1
b_0 (bar^{-1})	1154	1430	1180	1862.0
ΔH_0 (kJ mol^{-1})	22.6	28.8	21.41	44.5
n (/)	/	/	1.05	/
t_{h0} (/)	/	/	/	0.66
α (/)	/	/	/	0.71
SSE	123.8	127.5	119.8	103.6

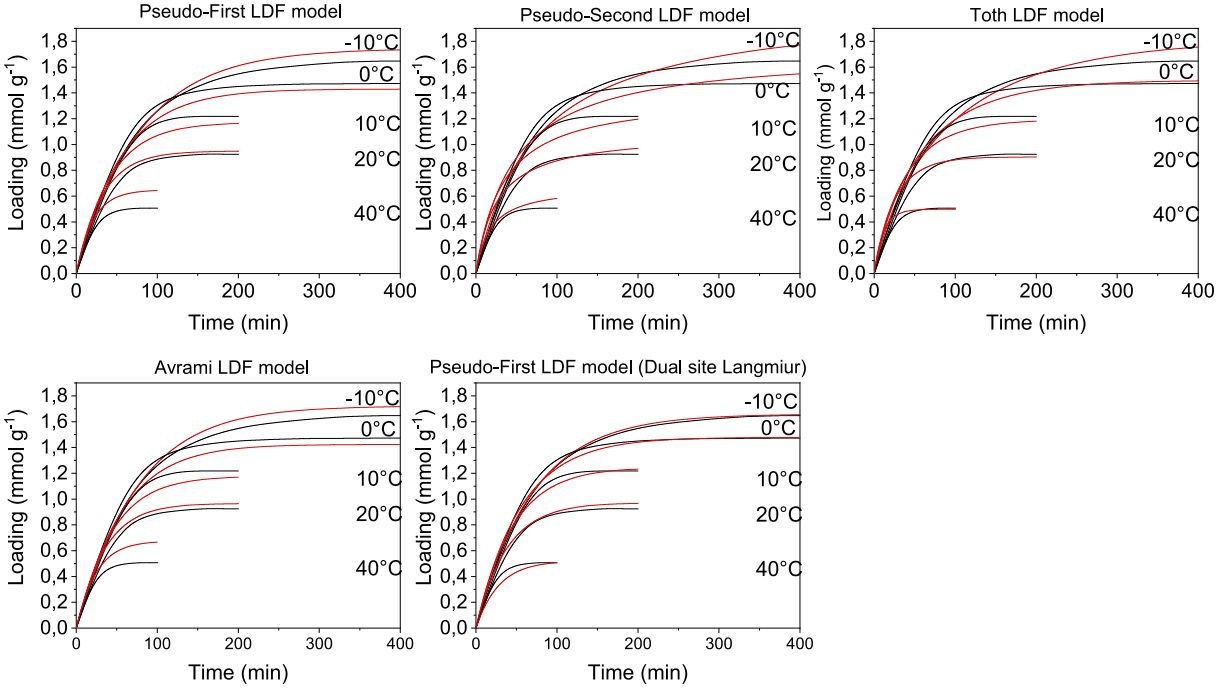

Fig. 6. Kinetic LDF models (red lines) compared to experimental breakthrough data (black lines) for CO_2 adsorption (400 ppm) on Lewatit® VP OC across a temperature range of −10 °C to 40 °C. The results indicate that among the models evaluated, the pseudo-first-order kinetic model coupled with a dual-site Langmuir isotherm yielded the best fit to the experimental breakthrough data.

Table 6
Pseudo-first kinetic model parameters using Dual-Site Langmuir isotherm for adsorption of CO_2 onto Lewatit® VP OC 1065 at $T_0 = 293.15$ K.

k_0 (min^{-1})	E_a (kJ mol^{-1})	$b_{0,1}$ (bar^{-1})	$\Delta H_{0,1}$ (kJ mol^{-1})	$b_{0,2}$ (bar^{-1})	$\Delta H_{0,2}$ (kJ mol^{-1})	$q_{s0,1}$ (mmol g^{-1})	$q_{s0,2}$ (mmol g^{-1})	SSE
0.02625	12.9	3112	46.44	$2.6*10^{-5}$	62.7	1.78	1.27	24.8

accurately describe the initial adsorption stages but over- or under-predicts CO_2 uptake at higher surface coverage. These findings align with previous studies, indicating that these models are only valid at low surface coverage and primarily describe the early stages of adsorption [52].

Comparing the pseudo-first order, pseudo-second order, and Avrami models, the latter was found to provide the best fit, not only for Lewatit® VP OC 1065, but also for PM01 [14], TRI-PEI-MCM41 [16] and PEI/SBA-15 [15] and TEPA/SBA-15 [15]. This model effectively represents multiple adsorption pathways [16]. The Toth model performed better than all others, though it still exhibited some deviation from the experimental data.

Bos et al. [17] also studied the intrinsic kinetics of Lewatit® VP OC 1065. Our calculated activation energies for the pseudo-first-order and pseudo-second-order models (18.8 and 36.4 kJ mol^{-1}, respectively) are in good agreement with their values (22.5 and 38 kJ mol^{-1}). However, our activation energy for the Tóth isotherm-based model was lower (5 kJ mol^{-1}) compared to their reported value of 15 kJ mol^{-1}. Similar to their findings, our analysis showed that the pseudo-first and pseudo-second-order LDF models poorly captured the experimental data, while the Tóth model provided the best overall fit among the three. These results are also consistent with the atomistic model, which shows that two amine groups must cooperate with the CO_2 molecule in order to bind it.

3.4.2. *Pseudo-first-order LDF model optimized with the dual-site Langmuir isotherm*

Building on the previous section, which demonstrated that dual-site adsorption best describes CO_2 behavior, we incorporated the dual-site Langmuir model into the pseudo-first adsorption rate equation to determine the adsorption equilibrium. This approach significantly improved the accuracy of the predictions, as reflected by a reduction in the SSE from above 100 to 24.8. The calculated activation energy of 12.9 kJ mol^{-1} aligns closely with the findings Bos et al. of 15.2 kJ mol^{-1}. While higher-order kinetic models may offer greater accuracy, they require more parameters, increasing computational costs. Furthermore, when humidity is considered, the number of parameters increases even further [19,53]. Therefore, when adopting more complex models, it is important to carefully evaluate whether the additional parameters are justified by a meaningful improvement in predictive performance.

However, all our models underestimated the isosteric heat of adsorption, which ranged between 20 and 60 kJ mol^{-1}. Unlike earlier studies that determined activation energy (E_a) and pre-exponential factor (k_0) from linearized Arrhenius plots and fitted each dataset separately, we fitted isotherm parameters, E_a, and k_0 simultaneously across all data. This integrated approach, incorporating temperature-dependent reaction rates, likely explains the deviations from previous models. Additionally, Bos et al. [17] studied flue gas, whereas our focus was on air capture, which might contribute to the differences in outcomes due to the different dominant adsorption mechanisms.

3.5. *Column dynamics*

All experimentally obtained breakthrough curves at inlet CO_2 concentrations of 400, 800, 1200, 1600, and 2000 ppm, measured at adsorption temperatures of −10 °C, 0 °C, 10 °C, 20 °C, and 40 °C, are provided in the Supplementary Information (Fig. S3). Immediate breakthrough occurs as a result of the short gas–sorbent contact time and the limited length of the packed bed.

A one-dimensional transport equation was used to describe the breakthrough curves, accounting for convection, axial dispersion, and adsorption onto the solid phase. Adsorption kinetics were modeled using a pseudo-first-order LDF approach, with equilibrium described by the dual-site Langmuir isotherm, which was shown in previous sections to provide the best fit across the studied cases. This aligns with previous findings indicating that, in amine-functionalized adsorbents where diffusion within the amine phase partially limits uptake, adsorption is best described by a dual-site mass transfer model: one site accounting for fast pore diffusion and the other for slower diffusion through the amine layer [54].

This model assumes constant gas velocity and axial dispersion coefficient along the reactor length, as well as negligible pressure drop. A one-dimensional model was selected because no significant differences between one-dimensional and two-dimensional modeling were observed [55]. Sorbent data, fixed-bed data and operating conditions are presented in Table 7. By solving a set of partial differential equations (PDE) using Matlab software, the breakthrough curves and concentration profiles for both gas (Fig. 7) and adsorbed phase (Fig. 8) can be obtained. For all experiments, the agreement between experimental and modeled results is strong, particularly given the complexity and size of the dataset, as indicated by an R^2 of 0.902.

As an initial assumption in the LDF models, the CO_2 concentration within the reactor was considered uniform and equal to the inlet concentration. In reality, at any position beyond the inlet ($L > 0$), the CO_2 concentration inside the reactor decreases from the inlet value until equilibrium is reached. This occurs because CO_2 is selectively adsorbed by the sorbent, leading to a reduction in gas-phase concentration and a corresponding increase in CO_2 loading on the particles. Consequently, the initial assumption overestimates both the CO_2 concentration and the adsorption capacity [33]. Having established the most suitable LDF model for describing the kinetics, the next step is to enhance its accuracy by updating the gas concentration profile by discretizing the reactor along its length. Therefore, the local CO_2 partial pressure is determined at each spatial point and time step. The sorbent uptake rate therefore considers the local CO_2 partial pressure, which refers to the actual gas-phase pressure at a specific position and time within the fixed bed, rather than the equilibrium partial pressure used in isotherm models.

Table 7
Parameters of the packed bed adsorber and operating conditions.

		Value	Reference
Sorbent data	Particle density	880 kg m^{-3}	[33]
	Porosity of the adsorbent particles	0.23	[25]
	Radius of the adsorbent particles	341 μm	
Fixed-bed data	Bed porosity (ε_b)	0.284	[29]
	Reactor diameter (d)	0.01 m	
	Length of the bed (L)	3 mm	
	Axial dispersion coefficient (D_{ax})[a]	1.2×10^{-4} m^2 s^{-1}	
Operation data	Gas phase superficial velocity	0.0148 m s^{-1}	
	Gas phase interstitial velocity	0.052 m s^{-1}	
	Operating pressure	1 atm	
	Operating adsorption temperature	−10, 0, 10, 20, 40 °C	

[a] Obtained from model fitting to the experimentally measured breakthrough curves.

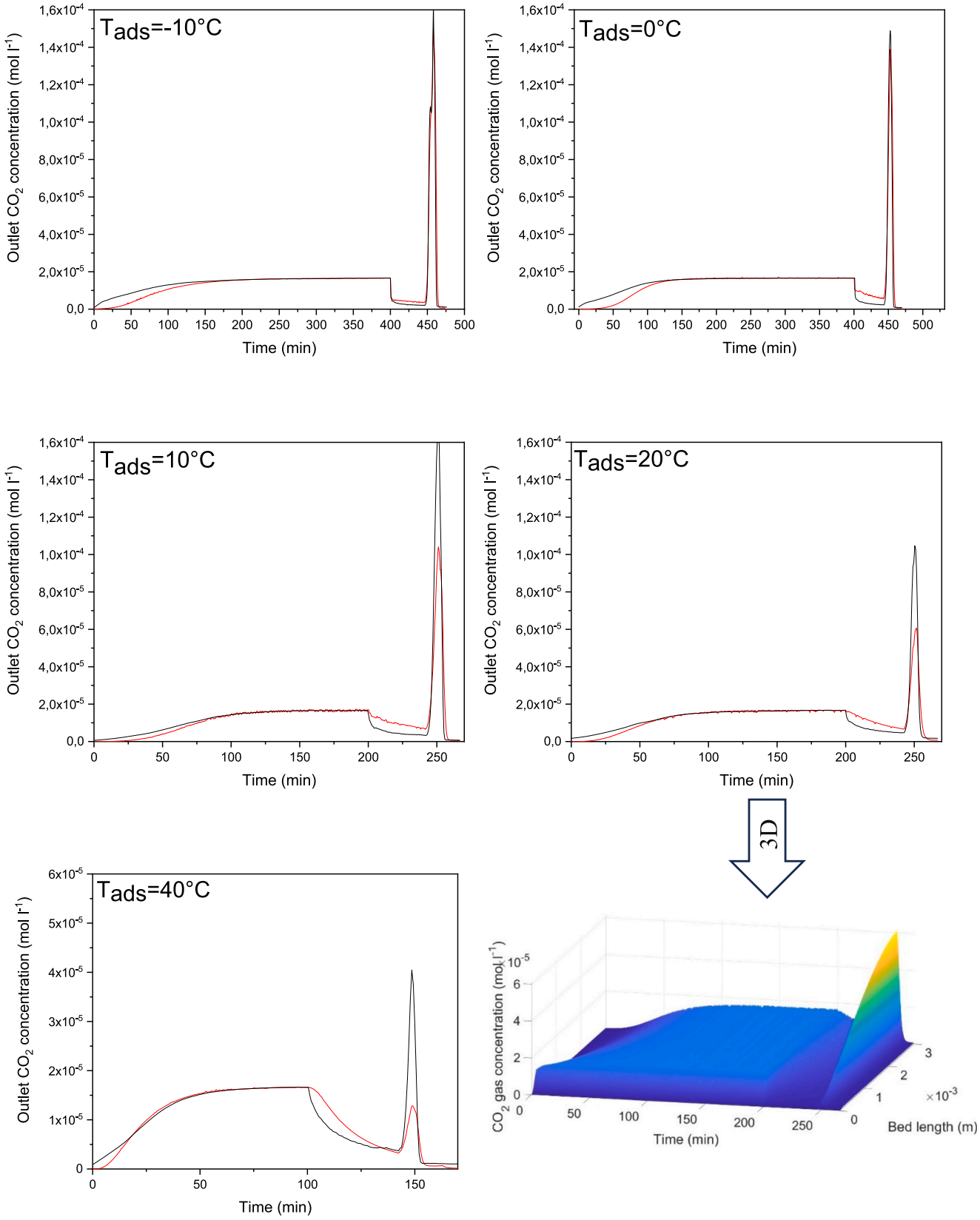

Fig. 7. CO_2 concentration profiles in the bulk phase (red line) obtained from model fitting to the experimentally measured breakthrough curves (black line) at an inlet CO_2 concentration of 400 ppm and adsorption temperature range of −10 °C to 40 °C, illustrating the breakthrough behavior and overall adsorption kinetics.

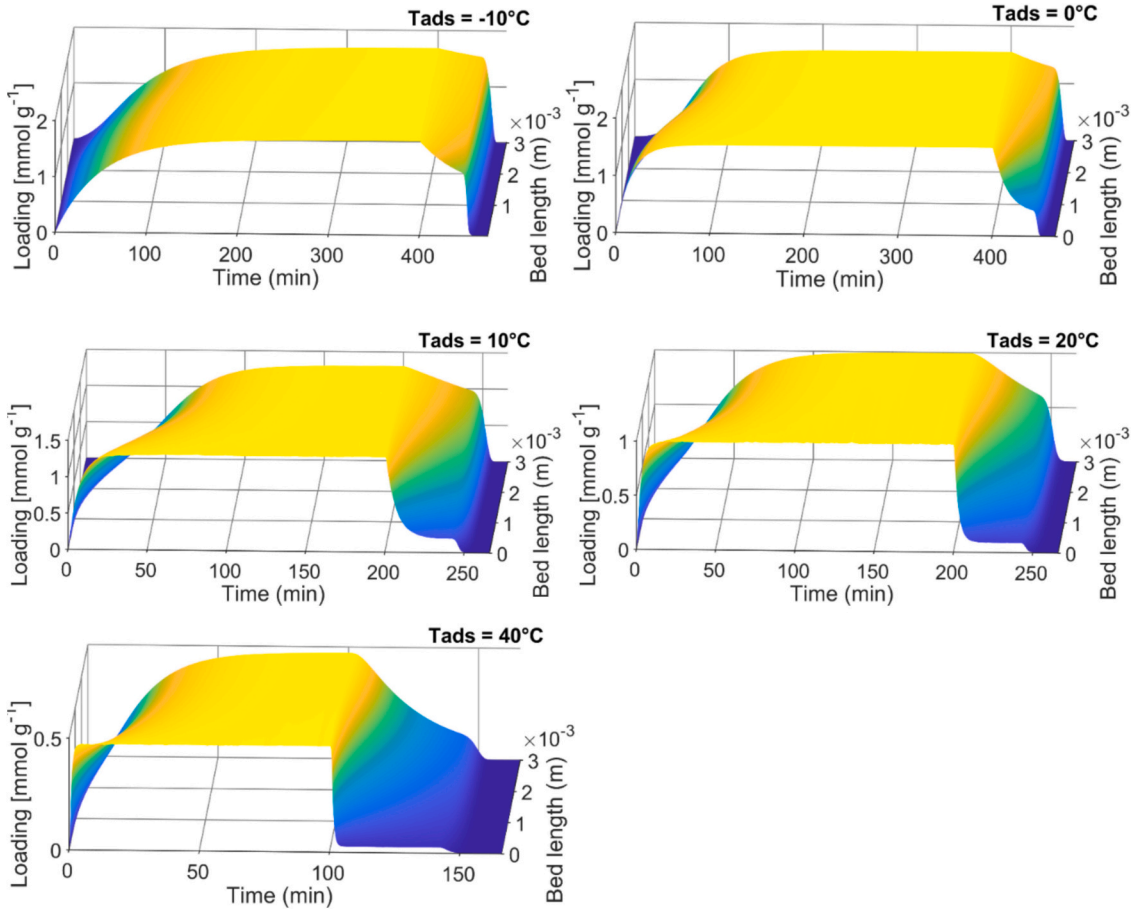

Fig. 8. CO_2 loading onto Lewatit® VP OC 1065 across a temperature range of −10 °C to 40 °C, at an inlet CO_2 concentration of 400 ppm. Breakthrough curves were modeled using a one-dimensional transport equation resolved in both time and spatial coordinates, accounting for convection, axial dispersion, and adsorption onto the solid phase.

3.5.1. Mass transfer coefficient

Balasubramaniam et al. [56] demonstrated that CO_2 adsorption kinetics are critical for process performance. Their parametric study showed that while the mass transfer coefficient has a minimal impact on minimum specific energy, sorption kinetics strongly affect productivity.

Fig. 7 shows the CO_2 concentration at the column outlet as a function of time, reflecting the breakthrough behavior and overall kinetics of the adsorption process. Fig. 8 complements this by showing the CO_2 loading on the sorbent over time, providing direct insight into how quickly the material captures CO_2 and reaches equilibrium. Higher temperatures generally accelerate mass transfer by increasing molecular motion, leading to faster initial uptake and earlier breakthrough in Fig. 7, while potentially reducing the ultimate sorbent loading observed in Fig. 8 due to weaker binding. Conversely, lower temperatures may slow adsorption kinetics but allow higher ultimate loading. Overall, higher mass transfer coefficients improve sorbent productivity by shortening the time required to reach target CO_2 loading during the adsorption step. In this study, the mass transfer rate constant was determined to be 0.0061 min^{-1} at 20 °C. Chemisorbents (SI-AEATPMS and APDES-NFC-FD) typically exhibited lower adsorption rate constants compared to physisorbents (MOFs), indicating higher mass transfer resistance. The values obtained in our work are lower than those typically reported for amine-functionalized sorbents (0.02–0.2 min^{-1}) [21,22,57], further highlighting the influence of moisture [53].

3.5.2. Activation energy

The fitted activation energy of 61.2 kJ mol^{-1} was validated by our DFT calculations. The activation *energy* predicted by the atomistic model is assessed to be 62.7 kJ mol^{-1} relative to the physisorbed state and 34.7 kJ mol^{-1} relative to unbound CO_2 (low partial pressure limit). This is notably higher than the activation energies reported by Bos et al. [17], who modeled diffusion and reaction within spherical particles of Lewatit® VP OC 1065 and found values ranging from 15 to 40 kJ mol^{-1}. However, the study was conducted at elevated CO_2 concentrations (5–20 % in N_2). At lower CO_2 concentrations, such as 400 ppm, higher activation energies are expected due to the shift toward more selective chemisorption, which involves stronger interactions and higher energy barriers.

Moreover, unlike previous studies that calculated activation energy (E_a) and pre-exponential factor (k_0) from the linearized Arrhenius equation, we simultaneously fitted isotherm parameters, E_a and k_0. While previous methods involved fitting each dataset separately, our model optimized all data collectively. This approach, which also accounts for temperature dependence of reaction rates, may explain the observed deviations from the modeled results.

The E_a reported earlier in this study is obtained from simplified kinetic models, where adsorption is described by the linear driving force expression and the rate constant follows an Arrhenius-type temperature dependence. This activation energy reflects the intrinsic or microscale kinetics of adsorption, typically under idealized conditions without spatial gradients or transport effects. It focuses purely on surface kinetics.

In contrast, E_a reported in this chapter is a part of a macroscale or process-level model describing a temperature swing adsorption process, which incorporates gas-phase mass balances accounting for convection, axial dispersion, and both adsorption and desorption kinetics. In this

more complex setting, k still follows the Arrhenius-type dependence, and E_a is extracted by fitting the entire column response. The resulting activation energy represents an effective value influenced by not only intrinsic adsorption kinetics but also macroscopic transport resistances such as mass transfer limitations. Therefore, while both activation energies are based on the same LDF framework, they capture different aspects of the system: the former characterizes material behavior and the latter reflects process-level performance.

4. Conclusions

The primary objective of this study was to identify and validate the most effective predictive model for fixed-bed adsorber dynamics. The system was simulated in MATLAB by fitting experimental data using a least-squares approach, and the results closely matched measurements, confirming the reliability of the modeling framework. The setup and procedures were carefully controlled, and repeated measurements yielded consistent data.

The results demonstrated that the dual-site Langmuir isotherm outperformed the commonly used Toth isotherm. The heat of adsorption determined from the dual-site isotherm model was calculated to be -69.8 kJ mol^{-1} for the high-energy sites and -50.0 kJ mol^{-1} for the low-energy sites, highlighting the importance of accounting for energetically distinct sites in amine-based sorbents. The total adsorption capacity, 3.32 mmol g^{-1}, closely agreed with elemental analysis, further validating the model.

A one-dimensional transport equation was further used to describe the breakthrough curves, incorporating convection, axial dispersion, and adsorption onto the solid phase. Adsorption kinetics were captured using a pseudo-first-order linear driving force model, with equilibrium described by the dual-site Langmuir isotherm, which provided the best fit across all studied cases. The rate constant was 0.0061 min^{-1} at 20 °C. While higher temperatures increase molecular motion and reduce sorption resistance, the kinetics ultimately limit CO_2 loading on the sorbent surface.

The activation energy obtained (61.2 kJ mol^{-1}) was higher than those reported in previous studies and showed a closer alignment with activation energies calculated via DFT analysis (35–60 kJ mol^{-1}), demonstrating the relevance of the multi-scale approach. DFT also provided a more detailed insight into the reaction mechanism, revealing the cooperating effect of two spatially adjacent amine groups in CO_2 chemisorption. While DFT was employed to decisively differentiate between the two possible mechanisms with regard to the participation of adjacent amino groups, the DFT-calculated energetics and kinetics require refining through experimental data because an atomistic model cannot capture the whole complexity of the sorbent. These values were therefore used as educated guesses for initial values in the fitting of the microkinetic model to experimental data. We show that CO_2 can physisorb either to the amine groups or, more weakly, to the non-polar aromatic surface. Chemisorption is due to the formation of a carbamate moiety.

Additionally, the study highlighted that lower temperature regions, often overlooked in existing literature, are critical for the Direct Air Capture (DAC) process. In contrast to the extensive research at ambient and higher temperatures, this study focused on the lower temperature range, which is more relevant to DAC applications. Previous studies have demonstrated that isotherms often underpredict adsorption capacities at temperatures below 20 °C. Expanding the temperature range used for model fitting improves the accuracy of calculated values by providing a broader set of reference data, thereby reducing deviations at lower temperatures, as also reflected by the slightly different results obtained in this study.

While the study provided valuable insights into the dynamics of CO_2 adsorption, it also acknowledged the influence of other absorbable solutes in multicomponent systems, which were outside the scope of this investigation but will be addressed in future work. Furthermore, a more detailed exploration of the influence of water on the adsorption process remains a necessary direction for future research.

CRediT authorship contribution statement

Dana Marinič: Writing – original draft, Visualization, Methodology, Investigation, Formal analysis, Data curation, Conceptualization. **Žan Lavrič:** Formal analysis. **Matej Huš:** Writing – review & editing, Writing – original draft, Formal analysis, Data curation. **Janvit Teržan:** Supervision, Methodology, Investigation. **Blaž Likozar:** Writing – review & editing, Supervision, Resources, Funding acquisition, Conceptualization.

Declaration of competing interest

The authors declare the following financial interests/personal relationships which may be considered as potential competing interests: Blaz Likozar reports financial support was provided by Slovenian Research and Innovation Agency. If there are other authors, they declare that they have no known competing financial interests or personal relationships that could have appeared to influence the work reported in this paper.

Acknowledgement

This research was funded by the Slovenian Research and Innovation Agency (ARIS) through core funding P2–0152, infrastructure funding I0-0039, and the research projects J7-4638, N2-0291 and N2-0310. This research was co-funded in the HyBReED project, supported by the European Union – NextGenerationEU. D.M. gratefully acknowledges the support of the U.S. Department of State and the Public Scholarship, Development, Disability, and Maintenance Fund of the Republic of Slovenia for the Fulbright scholarship, which enabled her research stay at the Center for Negative Carbon Emissions at Arizona State University. Computational facilities were provided in the framework of the HPC RIVR consortium and EuroHPC JU at the HPC system Vega at the Institute of Information Science, Maribor, Slovenia under project ID S25O02-04. The authors also extend their sincere thanks to Dr. Klaus Lackner for his valuable time and insightful discussions on the modeling approach.

Appendix A. Supplementary data

Supplementary data to this article can be found online at https://doi.org/10.1016/j.cej.2025.169895.

Data availability

Data will be made available on request.

References

[1] Q. Yu, D.W.F. Brilman, Design strategy for CO2 adsorption from ambient air using a supported amine based sorbent in a fixed bed reactor, Energy Procedia 144 (2017) 6102–6114, https://doi.org/10.1016/j.egypro.2017.03.1747.
[2] Xin Lan, NOAA/GML (gml.noaa.gov/ccgg/trends/) and Dr. Ralph Keeling, Scripps Institution of Oceanography (scrippsco2.ucsd.edu/).
[3] IPCC, in: Intergovernmental Panel on Climate Change (Ed.), Global Warming of 1.5 °C: Summary for Policymakers. In: Global Warming of 1.5 °C. An IPCC Special Report, 2018.
[4] W. Buijs, S. De Flart, Direct air capture of CO2 with an amine resin: a molecular modeling study of the CO2 capturing process, Ind. Eng. Chem. Res. 56 (2017) 12297–12304, https://doi.org/10.1021/acs.iecr.7b02613.
[5] C. Drechsler, D.W. Agar, Characteristics of DAC operation within integrated PtG concepts, Chem. Eng. J. 105 (2021) 103230, https://doi.org/10.1016/j.ijggc.2020.103230.
[6] M.J. Bos, S.R.A. Kersten, D.W.F. Brilman, Wind power to methanol: renewable methanol production using electricity, electrolysis of water and CO2 air capture, Appl. Energy 264 (2020) 114672, https://doi.org/10.1016/j.apenergy.2020.114672.

[7] W. Brilman, L. Garcia Alba, R. Veneman, Capturing atmospheric CO2 using supported amine sorbents for microalgae cultivation, Biomass Bioenergy 53 (2013) 39–47, https://doi.org/10.1016/j.biombioe.2013.02.042.

[8] C. Gebald, J.A. Wurzbacher, P. Tingaut, T. Zimmermann, A. Steinfeld, Amine-based nanofibrillated cellulose as adsorbent for CO 2 capture from air, Environ. Sci. Technol. 45 (2011) 9101–9108, https://doi.org/10.1021/es202223p.

[9] M. Ozkan, S.P. Nayak, A.D. Ruiz, W. Jiang, Current status and pillars of direct air capture technologies, IScience 25 (2022) 103990, https://doi.org/10.1016/j.isci.2022.103990.

[10] H. Bouaboula, J. Chaouki, Y. Belmabkhout, A. Zaabout, Comparative review of direct air capture technologies: from technical, commercial, economic, and environmental aspects, Chem. Eng. J. 484 (2024) 149411, https://doi.org/10.1016/j.cej.2024.149411.

[11] H.M. Schellevis, J.D. De La Combé, D.W.F. Brilman, An optimization framework for a temperature-vacuum swing adsorption direct air capture process, in: 16th International Conference on Greenhouse Gas Control Technologies, GHGT-16, Oct 23-27 2022 (Lyon, France).

[12] N. Casas, J. Schell, R. Pini, M. Mazzotti, Fixed bed adsorption of CO2/H2 mixtures on activated carbon: experiments and modeling, Adsorption 18 (2012) 143–161, https://doi.org/10.1007/s10450-012-9389-z.

[13] L.H. de Oliveira, J.G. Meneguin, E.A. da Silva, M.A.S.D. de Barros, P.A. Arroyo, W. M. Grava, J.F. do Nascimento, Linear driving force model in carbon dioxide capture by adsorption, Appl. Mech. Mater. 830 (2016) 38–45, https://doi.org/10.4028/www.scientific.net/amm.830.38.

[14] A.A. Al-Absi, M. Mohamedali, A. Domin, A.M. Benneker, N. Mahinpey, Development of in situ polymerized amines into mesoporous silica for direct air CO2 capture, Chem. Eng. J. 447 (2022) 137465, https://doi.org/10.1016/j.cej.2022.137465.

[15] Y. Miao, Z. He, X. Zhu, D. Izikowitz, J. Li, Operating temperatures affect direct air capture of CO2 in polyamine-loaded mesoporous silica, Chem. Eng. J. 426 (2021) 131875, https://doi.org/10.1016/j.cej.2021.131875.

[16] R. Serna-Guerrero, A. Sayari, Modeling adsorption of CO2 on amine-functionalized mesoporous silica. 2: kinetics and breakthrough curves, Chem. Eng. J. 161 (2010) 182–190, https://doi.org/10.1016/j.cej.2010.04.042.

[17] M.J. Bos, T. Kreuger, S.R.A. Kersten, D.W.F. Brilman, Study on transport phenomena and intrinsic kinetics for CO2 adsorption in solid amine sorbent, Chem. Eng. J. 377 (2019) 120374, https://doi.org/10.1016/j.cej.2018.11.072.

[18] T. Deschamps, M. Kanniche, L. Grandjean, O. Authier, Modeling of vacuum temperature swing adsorption for direct air capture using aspen adsorption, Clean Technol. 4 (2022) 258–275, https://doi.org/10.3390/cleantechnol4020015.

[19] J. Elfving, T. Sainio, Kinetic approach to modelling CO2 adsorption from humid air using amine-functionalized resin: equilibrium isotherms and column dynamics, Chem. Eng. Sci. 246 (2021) 116885, https://doi.org/10.1016/j.ces.2021.116885.

[20] W. Jung, K.S. Lee, Isotherm and kinetics modeling of simultaneous CO2 and H2O adsorption on an amine-functionalized solid sorbent, J. Nat. Gas Sci. Eng. 84 (2020) 103489, https://doi.org/10.1016/j.jngse.2020.103489.

[21] G. Leonzio, P.S. Fennell, N. Shah, A comparative study of different sorbents in the context of Direct Air Capture (DAC): evaluation of key performance indicators and comparisons, Appl. Sci. 12 (2022) 2618, https://doi.org/10.3390/app12052618.

[22] V. Stampi-Bombelli, M. van der Spek, M. Mazzotti, Analysis of direct capture of CO2 from ambient air via steam-assisted temperature–vacuum swing adsorption, Adsorption 26 (2020) 1183–1197, https://doi.org/10.1007/s10450-020-00249-w.

[23] J.A. Wurzbacher, C. Gebald, S. Brunner, A. Steinfeld, Heat and mass transfer of temperature-vacuum swing desorption for CO2 capture from air, Chem. Eng. J. 283 (2016) 1329–1338, https://doi.org/10.1016/j.cej.2015.08.035.

[24] L.A. Darunte, T. Sen, C. Bhawanani, K.S. Walton, D.S. Sholl, M.J. Realff, C. W. Jones, Moving beyond adsorption capacity in design of adsorbents for CO2 capture from ultradilute feeds: kinetics of CO 2 adsorption in materials with stepped isotherms, Ind. Eng. Chem. Res. 58 (2019) 366–377, https://doi.org/10.1021/acs.iecr.8b05042.

[25] R.T. Driessen, S.R.A. Kersten, D.W.F. Brilman, A thiele modulus approach for nonequilibrium adsorption processes and its application to CO2 capture, Ind. Eng. Chem. Res. 59 (2020) 6874–6885, https://doi.org/10.1021/acs.iecr.9b05503.

[26] H.M. Schellevis, T.N. van Schagen, D.W.F. Brilman, Process optimization of a fixed bed reactor system for direct air capture, Int. J. Greenh. Gas Control 110 (2021), https://doi.org/10.1016/j.ijggc.2021.103431.

[27] M. Rakesh Surati, J. Ning, Wei Chiu Supervisor Shareq Mohd Nazir, J. Ros Supervisor, Experimental Characterization of a Specific Chemisorbent and a Physisorbent for Direct Air Capture Application, Master's Thesis,, KTH Royal Institute of Technology, 2022.

[28] W.R. Alesi, J.R. Kitchin, Evaluation of a primary amine-functionalized ion-exchange resin for CO2 capture, Ind. Eng. Chem. Res. 51 (2012) 6907–6915, https://doi.org/10.1021/ie300452c.

[29] LANXESS AG, Technical Information: Lewatit® VP OC 1065, Technical Data Sheet.

[30] R.T. Driessen, J.J.Q. van der Linden, S.R.A. Kersten, M.J. Bos, D.W.F. Brilman, Characterization of mass transfer in a shallow fluidized bed for adsorption processes: modeling and supporting experiments, Chem. Eng. J. 388 (2020), https://doi.org/10.1016/j.cej.2019.123931.

[31] Q. Yu, J.D.L.P. Delgado, R. Veneman, D.W.F. Brilman, Stability of a benzyl amine based CO2 capture adsorbent in view of regeneration strategies, Ind. Eng. Chem. Res. 56 (2017) 3259–3269, https://doi.org/10.1021/acs.iecr.6b04645.

[32] V. Stampi-Bombelli, M. Mazzotti, Exploring geometric properties and cycle design in packed bed and monolith contactors using temperature-vacuum swing adsorption modeling for direct air capture, Ind. Eng. Chem. Res. 63 (2024) 19728–19743, https://doi.org/10.1021/acs.iecr.4c02303.

[33] R. Veneman, T. Hilbers, D.W.F. Brilman, S.R.A. Kersten, CO2 capture in a continuous gas-solid trickle flow reactor, Chem. Eng. J. 289 (2016) 191–202, https://doi.org/10.1016/j.cej.2015.12.066.

[34] Gaussian, Citation. https://gaussian.com/citation/ (accessed Aug. 16, 2025).

[35] Y. Zhao, N.E. Schultz, D.G. Truhlar, Design of density functionals by combining the method of constraint satisfaction with parametrization for thermochemistry, thermochemical kinetics, and noncovalent interactions, J. Chem. Theory Comput. 2 (2006) 364–382, https://doi.org/10.1021/ct0502763.

[36] N. Mardirossian, M. Head-Gordon, Thirty years of density functional theory in computational chemistry: an overview and extensive assessment of 200 density functionals, Mol. Phys. 115 (2017) 2315–2372, https://doi.org/10.1080/00268976.2017.1333644.

[37] A.D. McLean, G.S. Chandler, Contracted Gaussian basis sets for molecular calculations. I. Second row atoms, Z=11-18, J. Chem. Phys. 72 (1980) 5639–5648, https://doi.org/10.1063/1.438980.

[38] C. Peng, H.B. Schlegel, Combining synchronous transit and Quasi-Newton methods to find transition states, Isr. J. Chem. 33 (1993) 449–454.

[39] Duong D.Do., Adsorption Analysis: Equilibria and Kinetics vol. 2, Imperial College Press, London, 1998.

[40] R. Serna-Guerrero, Y. Belmabkhout, A. Sayari, Modeling CO2 adsorption on amine-functionalized mesoporous silica: 1. A semi-empirical equilibrium model, Chem. Eng. J. 161 (2010) 173–181, https://doi.org/10.1016/j.cej.2010.04.024.

[41] S. Lagergren, About the theory of so-called adsorption of soluble substances, Kungliga Svenska Vetenskapsakademiens Handlingar 24 (1898) 1–39.

[42] E.C.N. Lopes, F.S.C. Dos Anjos, E.F.S. Vieira, A.R. Cestari, An alternative Avrami equation to evaluate kinetic parameters of the interaction of Hg(II) with thin chitosan membranes, J. Colloid Interface Sci. 263 (2003) 542–547, https://doi.org/10.1016/S0021-9797(03)00326-6.

[43] M.J. Bos, T. Kreuger, S.R.A. Kersten, D.W.F. Brilman, Study on transport phenomena and intrinsic kinetics for CO2 adsorption in solid amine sorbent, Chem. Eng. J. 377 (2019) 120374, https://doi.org/10.1016/j.cej.2018.11.072.

[44] N. Álvarez-Gutiérrez, M.V. Gil, F. Rubiera, C. Pevida, Kinetics of CO2 adsorption on cherry stone-based carbons in CO2/CH4 separations, Chem. Eng. J. 307 (2017) 249–257, https://doi.org/10.1016/j.cej.2016.08.077.

[45] M.S. Shafeeyan, W.M.A. Wan Daud, A. Shamiri, A review of mathematical modeling of fixed-bed columns for carbon dioxide adsorption, Chem. Eng. Res. Des. 92 (2014) 961–988, https://doi.org/10.1016/j.cherd.2013.08.018.

[46] D.M. Ruthven, Principles of Adsorption and Adsorption Processes, John Wiley & Sons, New York, 1984.

[47] E. Sonnleitner, G. Schöny, H. Hofbauer, Assessment of zeolite 13X and Lewatit® VP OC 1065 for application in a continuous temperature swing adsorption process for biogas upgrading, Biomass Convers. Biorefinery 8 (2018) 379–395, https://doi.org/10.1007/s13399-017-0293-3.

[48] R. Veneman, N. Frigka, W. Zhao, Z. Li, S. Kersten, W. Brilman, Adsorption of H2O and CO2 on supported amine sorbents, Int. J. Greenh. Gas Control 41 (2015) 268–275, https://doi.org/10.1016/j.ijggc.2015.07.014.

[49] S. Sutanto, J.W. Dijkstra, J.A.Z. Pieterse, J. Boon, P. Hauwert, D.W.F. Brilman, CO2 removal from biogas with supported amine sorbents: first technical evaluation based on experimental data, Sep. Purif. Technol. 184 (2017) 12–25, https://doi.org/10.1016/j.seppur.2017.04.030.

[50] T. Watabe, K. Yogo, Isotherms and isosteric heats of adsorption for CO2 in amine-functionalized mesoporous silicas, Sep. Purif. Technol. 120 (2013) 20–23, https://doi.org/10.1016/j.seppur.2013.09.011.

[51] A.E. Rodrigues, C.M. Silva, What's wrong with Lagergreen pseudo first order model for adsorption kinetics? Chem. Eng. J. 306 (2016) 1138–1142, https://doi.org/10.1016/j.cej.2016.08.055.

[52] Y.S. Ho, Review of second-order models for adsorption systems, J. Hazard. Mater. 136 (2006) 681–689, https://doi.org/10.1016/j.jhazmat.2005.12.043.

[53] H.M. Schellevis, J.D. de la Combé, D.W.F. Brilman, Optimizing direct air capture under varying weather conditions, Energy Adv. 3 (2024) 1678–1687, https://doi.org/10.1039/d4ya00200h.

[54] Q. Grossmann, M. Mazzotti, Mass transfer of CO2 in amine-functionalized structured contactors in ultra-dilute conditions, Ind. Eng. Chem. Res. 64 (2025) 2339–2353, https://doi.org/10.1021/acs.iecr.4c04099.

[55] F.J. Gutiérrez Ortiz, M. Barragán Rodríguez, R.T. Yang, Modeling of fixed-bed columns for gas physical adsorption, Chem. Eng. J. 378 (2019), https://doi.org/10.1016/j.cej.2019.121985.

[56] B.M. Balasubramaniam, P.T. Thierry, S. Lethier, V. Pugnet, P. Llewellyn, A. Rajendran, Process-performance of solid sorbents for Direct Air Capture (DAC) of CO2 in optimized temperature-vacuum swing adsorption (TVSA) cycles, Chem. Eng. J. 485 (2024) 149568, https://doi.org/10.1016/j.cej.2024.149568.

[57] A. Sinha, L.A. Darunte, C.W. Jones, M.J. Realff, Y. Kawajiri, Systems design and economic analysis of direct air capture of CO2 through temperature vacuum swing adsorption using MIL-101(Cr)-PEI-800 and mmen-Mg2(dobpdc) MOF adsorbents, Ind. Eng. Chem. Res. 56 (2017) 750–764, https://doi.org/10.1021/acs.iecr.6b03887.